JACS
JOURNAL OF THE AMERICAN CHEMICAL SOCIETY
Article
pubs.acs.org/JACS

Mollenynes B–E from the Marine Sponge *Spirastrella mollis*. Band-Selective Heteronuclear Single Quantum Coherence for Discrimination of Bromo–Chloro Regioisomerism in Natural Products

Xiao Wang,[†] Brendan M. Duggan,[‡] and Tadeusz F. Molinski*[,†,‡]

[†]Department of Chemistry and Biochemistry, and [‡]Skaggs School of Pharmacy and Pharmaceutical Sciences, University of California, San Diego, 9500 Gilman Drive, MC-0358, La Jolla, California 92093-0358, United States

Supporting Information

ABSTRACT: Four new chlorobromohydrins, mollenynes B–E, were isolated from the marine sponge *Spirastrella mollis* collected from Hogsty Reef, Bahamas. Their structures were elucidated by integrated analysis of NMR, MS, and computational methods. A high-resolution band-selective HSQC experiment was developed to identify ^{13}C NMR signals in samples at the nanomole-scale that arise from Cl-substituted ^{13}C by exploiting the $^{35}Cl/^{37}Cl$ isotope shift.

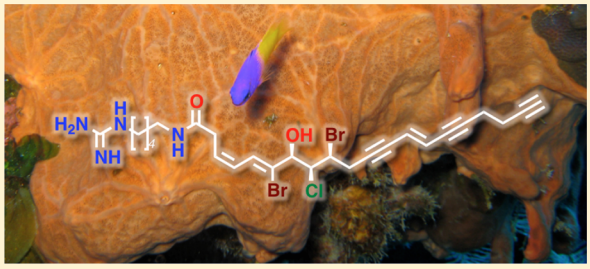

INTRODUCTION

Most natural products containing heterogeneous combinations of the halogens Cl and Br have been isolated from red algae (Rhodophyta) but infrequently from sponges (Porifera) or other marine invertebrates.[1] The enduring interest in these compounds lies in their diverse and profound biological activities.[2] Violacene (**1a**, Figure 1),[3] from *Plocamium violaceum*, and its acylic analog **1b**, from *P. cartilagineum*,[4] are two of dozens of polyhalogenated monoterpenes and lipids from red algae and sea hares that prey on them. In contrast, bromo–chloro compounds from sponges are rare and structurally diverse; they include bromo–chloro–cyclohexadienones from *Aplysina*,[5] bromotyrosine derivatives (e.g., wai'anaeamine A, **2**) from the Verongid sponges,[6] *Iotrochota purpurea*,[7] and *Suberea* sp.,[8] pyrrole–imidazole alkaloids axinellamines (**3**) from *Axinella* sp.,[9] tetrabromostyloguanidine from *Stylissa caribica*,[10] halogenated C-*nor*-D-*homo*-steroid nakiterpiosin (**4**) from *Terpios hoshinota*,[11] ω-bromochlorovinylidene azirines (*E*/*Z*-**5**) from *Dysidea fragilis*,[12] and most recently, the trihalogenated long-chain ene–yne carboxamide mollenyne A (**6**) from *Spirastrella mollis*.[13] Herein we report the discovery and structure elucidation of four new analogs, mollenynes B–E (**7**–**10**), from different specimens of the same sponge. The structure elucidation was completed by analysis of MS and NMR data, in particular, by refinement and application of a band-selective heteronuclear single quantum correlation (bsHSQC) 2D NMR experiment optimized for sensitivity down to the "nanomole-scale"[14] with sufficient power to resolve the $^{35}Cl/^{37}Cl$ isotope shift in the evolved ^{13}C dimension. The latter is an effective NMR tool for resolving bromo–chloro regioisomerism in polyhalogenated natural products, an outstanding problem that has led to erroneous assignments in the past in a number of polyhalogenated natural products.

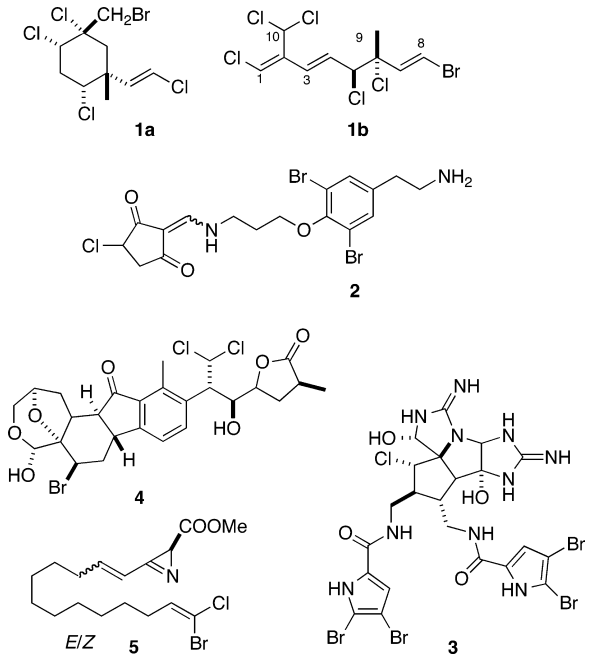

Figure 1. Chlorine–bromine containing marine natural products.

RESULTS AND DISCUSSION

Extracts of *Spirastrella mollis* from Plana Cays, Bahamas, exhibited antifungal activity in a disk-diffusion assay against *Candida albicans* and other pathogenic fungi. A survey (LCMS) of *S. mollis*, collected along a ~250 km arc from the Plana Cays to

Received: July 27, 2015
Published: September 3, 2015

DOI: 10.1021/jacs.5b07858
J. Am. Chem. Soc. 2015, 137, 12343–12351

Hogsty Reef, revealed **6** to be the major bromo-chlorinated diyne−ene component samples only from the former location. Samples of *S. mollis* from Hogsty Reef lacked **6** and contained new mollenyne analogs. Sequential solvent partitioning of the CH_3OH extract of one of the latter samples, followed by further purification by Sephadex LH-20 column chromatography and repeated reversed phase HPLC purification, afforded microgram quantities of **7**−**10** (0.16−0.57 ppm w/w).

The molecular formula of mollenyne B (**7**), $C_{26}H_{33}Br_2ClN_4O_2$, was established from HRESIMS data (*m*/*z* 627.0728 [M + H$^+$], Δmmu = 0.4) with one degree of unsaturation more than **6** (Figure 2). The ^{1}H NMR, DQF-COSY, HSQC, and HMBC

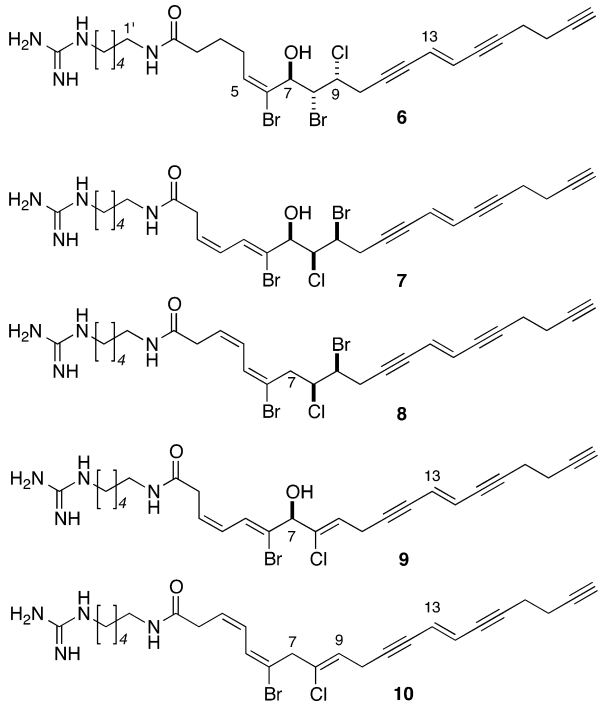

Figure 2. Structures of mollenynes A−E (**6**−**10**).

signals of C-10 to C-20 and the guanidine-terminated side chain of **7** were almost identical to those of **6** (Tables 1 and 2), confirming both **6** and **7** contained the homoagmatine residue. The vinyl C−H signals in the ^{1}H NMR spectrum of **7** (δ_H 5.92, m, 6.47, d, *J* = 10.7 Hz) confirmed the presence of an additional double bond, *Z*-Δ^3.

The geometry of the Δ^5-trisubstituted vinyl bromide in **7** was also assigned as *Z* based on the observation of 1D NOE and 2D NOESY cross-peaks between H-7 and H-5 (Figure 3), in contrast to **6** where a NOESY cross-peak between H-4 and H-7 supported an *E*-Δ^5 double bond. As in **6**, an HSQC cross-peak at H-7−C-7 (δ 4.47, 79.4 ppm) revealed the presence of the C-7 hydroxyl group in **7**; however, assignment of both regiochemistry and stereochemistry at C-8 to C-9 was made more challenging by two factors. The locations of Cl and Br at the sp^3-stereocenters were ambiguous because the corresponding ^{1}H and ^{13}C NMR chemical shifts of CH-8 and CH-9 were almost identical (e.g., **6**; δ_{H8}, δ_{H9} = 4.57 ppm; δ_{C8} = 59.3 ppm and δ_{C9} = 59.4 ppm),[13] and differences in vicinal *J* values between **6** and **7** suggested possibly different relative configurations. Based solely on interpretation of ^{13}C NMR chemical shifts, it appeared that the halogen atoms in **7** had swapped positions with respect to **6**. In order to verify this unusual finding, we sought independent evidence. For mollenyne A (**6**), the problem was solved by conversion of the natural product to C-7−C-8 epoxide **6a** (Scheme 1, saturation of the carbon−carbon double and triple bonds with concomitant hydrogenolysis of the C-6 Br group, H_2, Pd−C), containing only one Cl. Because formation of the *trans*-epoxide **6a** resulted from intramolecular S_N2 substitution of a vicinal bromohydrin with S_N2 inversion at C-8, an *erythro* C-7, C-8 relationship was established for **6**.[13] Independently, the C-8 configuration was relayed to C-9 by *J*-based analysis using data obtained from HECADE[15] and *J*-resolved HMBC experiments.[16] When attempts were made to apply the same procedure to **7**, epoxide formation failed and only decomposition was observed because of lability of the starting material to base, even as mild as K_2CO_3 or Ag_2O.

In many contiguous dihalohydrin systems (mollenynes A (**6**) and B (**7**) included) differentiation of the Cl-substituted ^{13}C NMR signals from those containing Br carbons, based solely on ^{1}H or ^{13}C chemical shifts, is unreliable because of similarity of the chemical shifts; however, in optimal cases Cl-substituted ^{13}C signals can be identified by exploiting the ^{37}Cl/^{35}Cl isotope shift in ^{13}C NMR.[17] For example, the isotope shifts of the order of $\Delta\nu$ = 0.6−0.9 Hz ($\Delta\delta$ 5−7 ppb on a 125 MHz ^{13}C spectrometer) have been observed in chloromethanes.[18] Unfortunately, the available quantity of **7** (~43 μg) was insufficient for directly detected ^{13}C NMR spectroscopy. In order to overcome this limitation, we developed a refinement of band-selective high-resolution 2D HSQC (bsHSQC)[19] for indirect detection of ^{35}Cl/^{37}Cl isotope shifts. Briefly, digital filtering was used to restrict the ^{1}H sweep width and a band-selective "soft" excitation ^{13}C pulse was employed to excite only the ^{13}C resonances in the region of interest. Ultrahigh resolution in F1 was achieved by narrowing the evolved dimension to only a few ppm and increasing the number of increments, thereby achieving a spectroscopic discrimination in ^{13}C (F1) comparable to the absolute magnet resolution ($\Delta\nu \approx 0.1$−0.3 Hz/point' see Supporting Information for technical details).[20] The combination of these refinements led to acquisition of 2D data in reasonable time scales, while the use of a cryomicroprobe NMR at 600 MHz lowered the detection limit to samples down to approximately a few 10s of μg (~69 nmol of **7**).

In the event, measurement of bsHSQC of **7** (Figure 4) revealed a ^{35}Cl/^{37}Cl isotope shift, split cross-peak for H-8 and C-8 (δ_H 4.49 and δ_C 66.7 ppm) with a shoulder resolved from the major signal ($\Delta\nu \approx 0.9$ Hz). In contrast, the H-9−C-9 cross peak and corresponding slice was symmetrical (Figure 4c,d). A more accurate estimation of the chemical shifts of the isotopically shifted ^{13}C signals was obtained by deconvolution of a slice taken through the HSQC cross-peak (^{13}C dimension, Figure 4b) by least-squares fitting of the sum of two Lorentzian peaks to the experimental data, via optimization of peak positions, line widths, and intensities (Table 3). The major peak was centered at δ 66.7043 ppm, due to ^{35}Cl−^{13}C, and a minor component at δ 66.6966 ppm from ^{37}Cl−^{13}C ($\Delta\delta$ = 0.0076 ppm or $\Delta\nu$ = 1.2 Hz at 150 MHz). The dominant component has a larger line width ($w_{1/2}$ = 0.86 ± 0.02 Hz) than the minor component ($w_{1/2}$ = 0.68 ± 0.05 Hz) as would be expected from the larger quadrupolar broadening of ^{13}C by the lighter isotope (^{35}Cl, *I* = 3/2, *Q* = -1.0×10^{-29} Q·m^{-2}; ^{37}Cl, *I* = 3/2, *Q* = -7.9×10^{-30} Q·m^{-2}).[21] The extracted integral ratio of the two components was 0.305 ± 0.05, which is consistent with the natural abundance ratio of ^{37}Cl/^{35}Cl in seawater.[22] Thus, ^{37,35}Cl was located unambiguously at C-8, and by deduction, Br was placed at C-9.

For comparison purposes, we measured both bsHSQC and high-resolution ^{13}C NMR of a more abundant natural product,

DOI: 10.1021/jacs.5b07858
J. Am. Chem. Soc. 2015, 137, 12343−12351

Table 1. ^{1}H NMR (600 MHz, CD_3OD) Results of Mollenyne A (6)[13] and New Mollenynes B–E (7–10)

	δ_H in ppm, m (J in Hz)				
no.	6	7	8	9	10
2	2.23, t (7.4)	3.18, m	3.10, m	3.17, m	3.11, dd (7.7, 1.5)
3	1.79, m	5.92, m	5.74, m	5.85, m	5.73, m
4	2.23, m	6.47, t (10.7)	6.36, t (11.4)	6.45, t (10.7)	6.35, tt (11.5, 1.5)
5	6.10, t (7.7)	7.09, d (10.6)	6.99, d (11.4)	7.09, d (10.5)	6.99, d (11.5)
7	4.73, d (9.7)	4.47, d (7.6)	3.25, m	4.87,[a] s	3.67, s
			3.11, m		
8	4.57, m	4.49, dd (7.6, 2.5)	4.66, ddd (7.7, 5.9, 1.8)		
9	4.57, m	4.16, ddd (8.4, 6.1, 2.5)	4.42, ddd (8.2, 6.4, 1.8)	6.08, t (6.8)	5.77, t (6.7)
10	2.97, m	3.15, m	3.11, m	3.30[a]	3.26, d (6.7)
		3.07, ddd (17.4, 6.1, 1.9)	3.07, m		
13	5.97, dt (16.1, 1.9)	5.97, dt (16.1, 2.0)	5.97, dt (16.0, 2.0)	5.91,[b] d (16.6)	5.91,[b] dt (16.4, 1.4)
14	5.91 (16.1, 2.0)	5.90, m	5.91, dt (16.0, 1.9)	5.90,[b] d (16.6)	5.89,[b] dt (16.4, 1.4)
17	2.54, td (7.2, 2.0)	2.54, td (7.1, 1.9)	2.54, td (7.2, 1.9)	2.54, t (7.0)	2.54, td (7.1, 1.4)
18	2.39, td (7.2, 2.6)	2.39, td (7.1, 2.6)	2.39, td (7.1, 2.6)	2.38, td (7.0, 2.4)	2.38, td (7.1, 2.6)
20	2.31, t (2.6)	2.31, t (2.6)	2.31, t (2.6)	2.31, t (2.4)	2.30, t (2.6)
1′	3.18, t (7.2)	3.19, m	3.19, t (7.1)	3.20, m	3.19, t (7.1)
2′	1.54, p (7.2)	1.54, p (7.4)	1.55, p (7.4)	1.55, p (7.4)	1.55, p (7.4)
3′	1.38, p (7.2)	1.38, p (7.4)	1.39, p (7.4)	1.39, p (7.4)	1.39, p (7.4)
4′	1.61, p (7.2)	1.61, p (7.4)	1.61, p (7.4)	1.61, p (7.4)	1.61, p (7.4)
5′	3.16, t (7.2)	3.16, m	3.16, t (7.1)	3.16, m	3.16, t (7.1)

[a]Obscured by solvent signals. [b]Partially resolved AB spin system.

Table 2. ^{13}C NMR (CD_3OD) Results of Mollenyne A (6)[13] and New Mollenynes B–E (7–10)[a]

	δ_C in ppm				
compd	6	7	8	9	10
1	175.6	172.5	172.8	173.4	172.7
2	36.4	36.4	35.7	36.5	35.8
3	26.3	130.7	127.7	129.7	127.3
4	30.3	128.1	126.4	128.9	126.2
5	137.3	127.8	131.9	125.7	131.3
6	128.5	129.2	125.0	129.5	124.9
7	70.8	79.4	43.7	80.0	45.8
8	59.3	66.7	62.1	135.0	132.2
9	59.4	52.5	54.6	124.5	124.8
10	29.6	28.5	28.5	19.3	19.8
11	89.9	90.1	90.4	91.3	91.2
12	82.6	82.5	82.2	79.9	79.6
13	122.6	122.4	122.5	121.6	121.4
14	120.7	120.4	120.6	121.6	121.4
15	80.4	80.0	80.0	80.2	80.0
16	94.6	94.4	94.4	93.8	93.5
17	20.4	20.1	20.0	20.1	20.1
18	19.2	19.0	18.8	19.0	18.9
19	83.3	82.9	83.0	82.9	82.8
20	70.5	70.0	70.5	70.5	70.5
1′	40.1	39.9	39.8	39.9	39.9
2′	30.1	29.7	29.7	29.7	29.7
3′	24.9	24.7	24.5	24.6	24.6
4′	29.4	29.1	29.1	29.1	29.1
5′	42.4	42.1	42.1	42.1	42.1
6′	158.6	158.2	158.2	158.8	158.1

[a]Obtained from both direct detected ^{13}C NMR and indirect detected experiments (HSQC, HMBC).

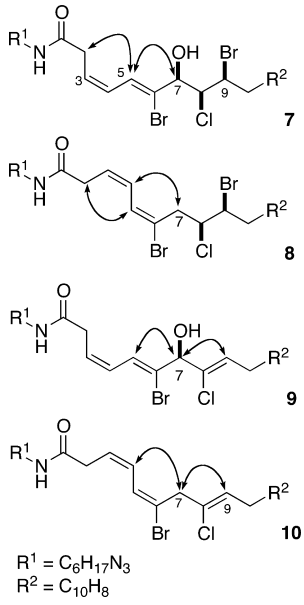

Figure 3. Selected NOESY correlations support the assigned double bond configurations of 7–10. See Figure 1 for complete structures.

the bromopentachloroterpene **1b** (Figure 5). As can be seen from the ^{13}C NMR spectrum of **1b**, each of the chlorinated carbons shows evidence of ^{35}Cl/^{37}Cl isotopic splitting. The largest isotope splitting effect is observed for the quaternary carbon, C-6 (δ 71.5, $\Delta\delta$ = 0.009 ppm), while the chlorovinyl signal C-1 (δ_C 119.6, CH, shoulder, estimated $\Delta\delta$ = 0.006 ppm) showed the smallest splitting. As expected, the dichloromethyl signal (δ 65.5, C-10) is split in a more complex manner because of the three possible isotopic permutations of two chlorine atoms, $^{35}Cl_2$, $^{35}Cl^{37}Cl$, and $^{37}Cl_2$ (abundance ratio, 9.8:6.3:1). The bsHSQC spectrum of **1b** reveals split cross-peaks for two of the three chlorinated H–C cross peaks. Interpretation of these split cross-peaks confirms the original assignment of the ^{1}H and ^{13}C NMR spectra of **1b** *independently* of empirical chemical shift increments. It should be noted that DFT calculations of NMR chemical shifts based on gauge-independent atomic orbital

DOI: 10.1021/jacs.5b07858
J. Am. Chem. Soc. 2015, 137, 12343–12351

Scheme 1[a]

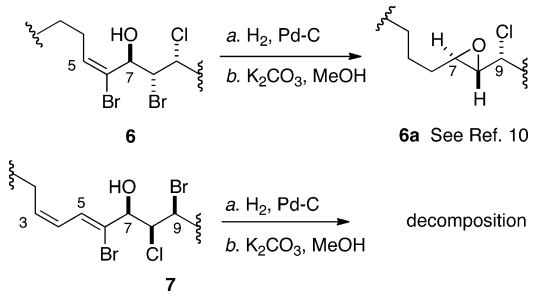

[a]See also ref 13.

methods GIAO (see below) are least accurate (and less reliable for assignment purposes) for Br-substituted carbons because of poor estimations of spin−orbit effects.[23]

To our knowledge, this is the first report exploiting the ^{35,37}Cl isotope shift to elaborate the constitution of a polyhalogenated natural product. In the present context, indirect detection of the ^{37,35}Cl isotope shifts from HSQC, as opposed to direct-detected ^{13}C NMR spectra, is remarkable because of the applicability to samples of natural products at the nanomole-scale. Quantitative deconvolution analysis of cross-peaks may have broader applications; for example, measurement of ^{35}Cl/^{37}Cl isotope fractionation during the biosynthesis of chlorinated natural products, which has traditionally relied on MS methods, milligram sample size, and obligatory degradative sample preparation.

Table 3. Values Used To Deconvolute the ^{13}C Slice through the H-9−C-9 HSQC Cross-Peak of 7

	major peak	minor peak
position (ppm)	66.7043 ± 0.0008	66.6966 ± 0.0023
line width (Hz)	0.86 ± 0.02	0.68 ± 0.05
intensity	129 000 ± 2607	50 000 ± 2890
integral[a]	2315 ± 101	705 ± 92

[a]The integral value was not fitted but was obtained from the line width and intensity values.

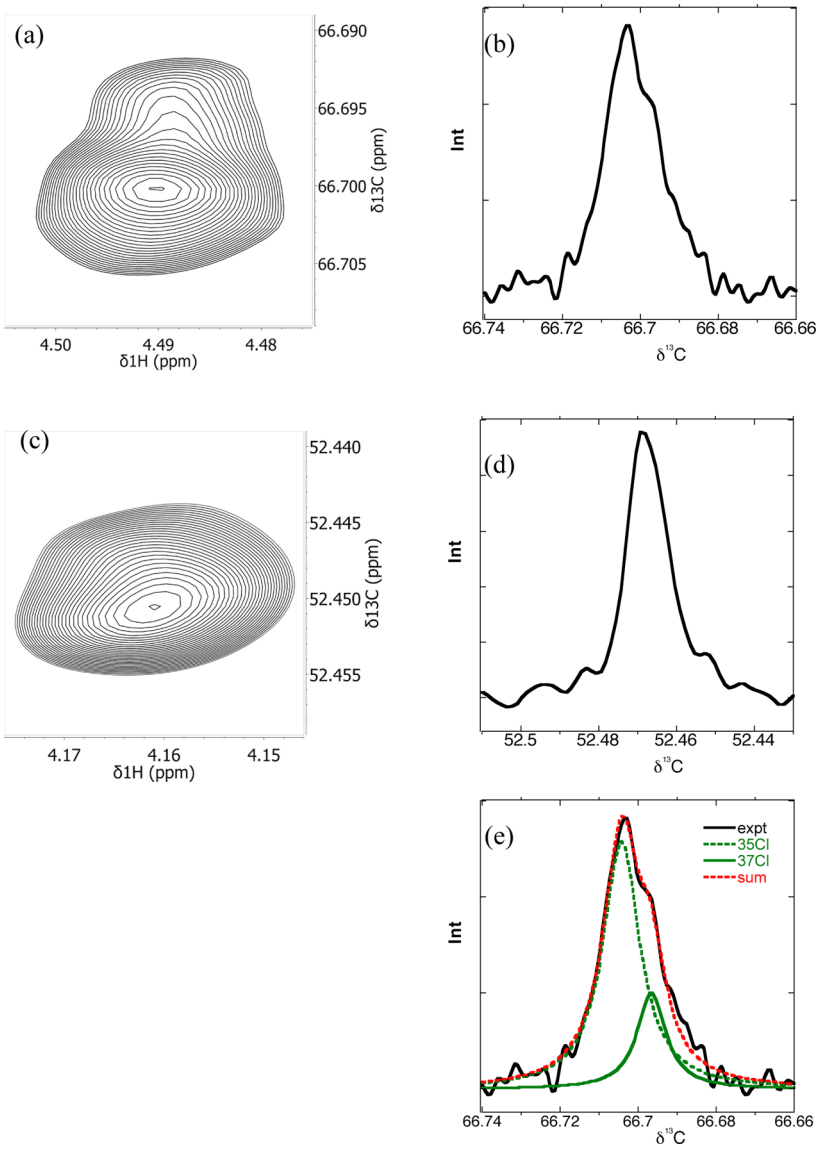

Figure 4. Band-selective high-resolution HSQC of 7 (600 MHz, CD_3OD) (see Experimental Section and Supporting Information for details of acquisition parameters): (a) H-8−C-8 cross-peak, (b) 1D slice (^{13}C) from (a), revealing a ^{35}Cl/^{37}Cl isotope shift, (c) H-9−C-9 cross-peak, (d) 1D slice (^{13}C) from (c), and (e) deconvolution and curve fitting of ^{35}Cl−C-8 and ^{37}Cl−C-8 components from (b).

DOI: 10.1021/jacs.5b07858
J. Am. Chem. Soc. 2015, 137, 12343−12351

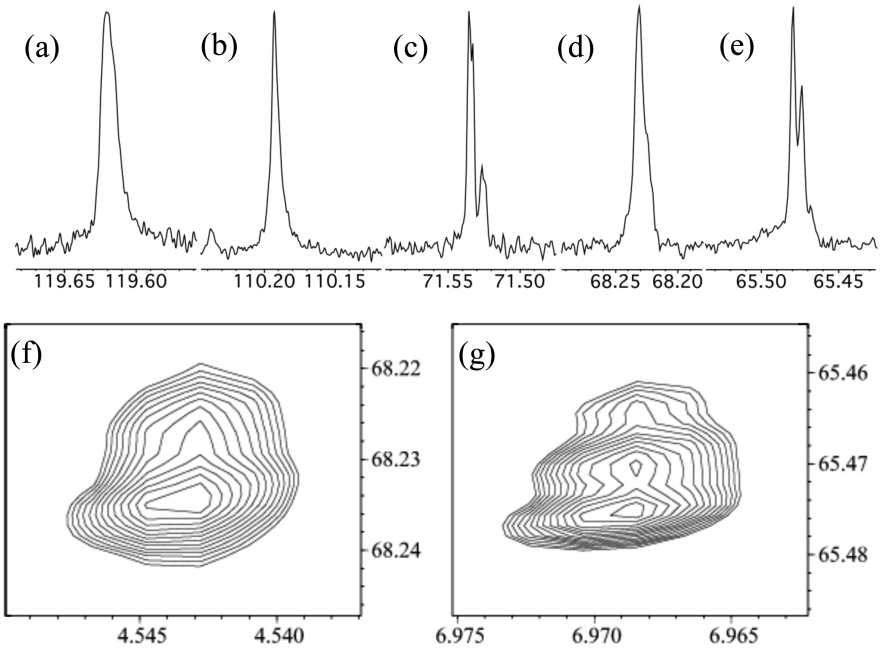

Figure 5. High-resolution ^{13}C NMR (125 MHz) and band-selective high-resolution HSQC (600 MHz) of **1b** (CD_3OD) (see Experimental Section and Supporting Information for details of acquisition parameters): (a) C-1 peak, (b) C-8 peak, (c) C-6 peak, (d) C-5 peak, (e) C-10 peak, (f) bsHSQC, C5−H5 cross-peak, (g) bsHSQC, C-10−H10 cross-peak.

Analysis of *J*-based coupling data was attempted in order to determine the relative configurations at C-7, C-8, and C-9.[16] Long-range $^{2,3}J_{CH}$ couplings were measured using a HETLOC experiment,[24] and $^{3}J_{HH}$ couplings were derived from both HETLOC and analysis of splitting patterns in ^{1}H NMR multiplets. Unfortunately, because of the small magnitude scalar coupling between H-8 and H-9 ($^{3}J_{HH}$ = 2.5 Hz), the relay of magnetization during the HETLOC experiment was weak and the key $^{3}J_{CH}$ coupling between H-8 and C-10 was not observed. Lack of sensitivity in the *J*-resolved HMBC of **7**, again, frustrated attempts to measure the value of $^{3}J_{CH}$. The available data were sufficient only to determine that H-9 was aligned *anti* to the Cl atom at C-8 as a consequence of the small magnitudes of vicinal H-9−C-8 coupling ($^{3}J_{CH}$ = 3.4 Hz) and H-8−H-9 ($^{3}J_{HH}$ = 2.5 Hz) couplings.

A solution to the stereoassignment of **7** was secured by computation, including DFT calculations of conformations, energies, and accurate ^{1}H NMR coupling constants. Kutateladze and Mukhina recently reported calculation of spin−spin coupling constants (J_{HH}) based on parametric scaling of calculated Fermi contacts (FCs), extended by a "minimalistic relativistic force field" and refined by critical selection of natural bond order (NBO) hydridization coefficients and atom connectivity.[25] Their second-generation DU8 basis set (developed from a training set of 475 spin−spin couplings) showed remarkable accuracy in predicting J_{HH} values when applied to a test set of 919 published experimental spin−spin couplings in synthetic compounds and natural products (σ = 0.29 Hz and a maximum unsigned error (mue) of not exceeding 1 Hz). In our initial reliability test of the DU8-based calculations, model compound **11** was employed to simulate the spin systems and known relative configuration of the bromochlorohydrin unit in **6**.

The geometries of conformers of **11** were first optimized by DFT (B3LYP/6-31G(d) level), followed by calculation of the coupling constants of each conformer using DU8 basis set[25b] (Table 4). Energies of each of the 30 lowest energy conformations were calculated, and the relevant coupling constants were determined after weighting by the Boltzmann distributions of the associated conformer populations (B3LYP/6-311+G(2d,p)).[26]

Table 4. Vicinal Coupling Constants ($^{3}J_{HH}$, Hz) of 6 and 7, Calculated Values (DFT) of Diastereomeric Models 11−15, and Differences[a]

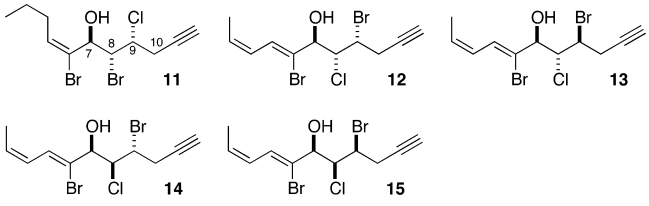

	6	11	7	12	13	14	15
H-7−H-8	9.6	9.3	7.6	8.7	8.6	3.4	7.3
$\Delta J_{H\text{-}7-H\text{-}8}$		−0.3		1.1	1.0	−4.2	−0.3
H-8−H-9	1.6	1.6	2.5	1.6	2.2	8.0	2.2
$\Delta J_{H\text{-}8-H\text{-}9}$		0		−0.9	−0.3	5.5	−0.3

[a]See text, Experimental Section, Supporting Information, and ref 25b for details.

The calculated $^{3}J_{HH}$ magnitudes for H-7−H-8 and H-8−H-9 **11** were in very good agreement with the experimental data of **6** (Table 4, column 2), although deviations between calculated and measured values for H-9−H-10 and H-9−H-10′ were evident due to strong coupling in this system and differences in the chain termini of the models (see Supporting Information). Mollenyne B (**7**) exhibited a vicinal coupling of medium magnitude for H-7−H-8 (^{3}J = 7.6 Hz) compared to the larger value in **6** (^{3}J = 9.6 Hz), indicating a distribution of *anti* and *gauche* conformers. Models **12**−**15**, representing all four possible diastereomers of **7**, were then built and minimized in the same manner as **11** (Table 4, columns 4−7). The (7*S*,8*S*,9*R*)-**14** showed a dominance of the *gauche* conformation, indicated by the small magnitude of the H-7−H-8 vicinal coupling (^{3}J = 3.4 Hz).

In contrast, alternative configurations represented by the stereotriads (7*S*,8*R*,9*R*)-**12** and (7*S*,8*R*,9*S*)-**13** have *anti* oriented

DOI: 10.1021/jacs.5b07858
J. Am. Chem. Soc. 2015, 137, 12343−12351

substituents at C-7 and C-8, resulting in a large magnitude H-7–H-8 coupling (^3J = 8.7 and ^3J = 8.6 Hz, respectively). Model (7*S*,8*S*,9*S*)-**15** matched most closely (rmsd error) with the experimental data of **7** (Figure 6). Thus, we assign the stereoconfiguration of **7** to be (7*S*,8*S*,9*S*).[27]

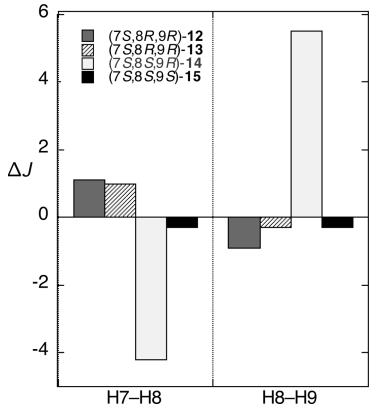

Figure 6. Calculated (DFT optimized geometries and DU8 basis set; see ref 25b and text) ^3J coupling constants differences (ΔJ) of diastereomeric models compounds (**12**–**15**) from measured values of mollenyne B (**7**).

With improvements in reliability and computational power, NMR chemical shifts calculated by ab initio methods based on GIAO[28] have found increased utility in natural product assignments.[29] Goodman and co-workers recently derived a method for stereochemical assignment based on computed NMR chemical shifts coupled with error analysis that delivers confidence limits of stereoassignment based on errors of each ^{1}H or ^{13}C chemical shift (the DP4 probability) rather than a correlation coefficient or mean absolute error.[30] Despite a limitation of accuracy in calculated NMR chemical shifts for Br-substituted ^{13}C and the attached ^{1}H signal, good to excellent predictions for chemical shifts were obtained for the up to 64 relative configurations of over 100 molecules, some embodying considerable structural complexity. Starting with our DFT minimized geometries of models **12**–**15**, we calculated NMR chemical shifts and the DP4 probabilities associated with each ^{1}H or ^{13}C chemical shift in each model (see Supporting Information, Tables S3 and S4) and evaluated the stereoassignment with that obtained from the *J*-based DU8 calculations (above). Model **15** from **12**–**15** was, again, the best match to **7** by ^{1}H or ^{13}C chemical shifts (when halo-substituted ^{13}C were excluded), although with somewhat lower confidence (e.g., DP4 for ^{13}C, 25.5%, 11.6%, 30.0%, and 33.0%, respectively).

Mollenyne D (**9**), with a molecular formula of $C_{26}H_{32}BrClN_4O_2$ (*m*/*z* 547.1467 [M + H$^+$], Δmmu = 0.3), is formally the product of *β*-elimination of HBr from mollenyne B (**7**). The ^{1}H NMR spectrum of **9** showed distinct differences from those of **6** and **7**. First, the ^{1}H NMR chemical shifts of H-13, H-14, and C-13, C-14 are almost coincident, resulting in an unresolved, single cross peak in HSQC for both signals and collapse of the AB spin system of **6** and **7** to a weakly resolved, strongly coupled AB pattern (δ 5.90 ppm, ^3J = 16.4 Hz). The large vicinal coupling constant confirmed the *E*-Δ^{13} double bond in **9**, as found in all mollenynes, to date. Second, in contrast to **6** and **7**, only one signal in the range δ 4–5 ppm was observed in the HSQC spectrum of **9** (δ 4.87, s, obscured by the CD_3OH peak in ^{1}H NMR). This downfield shifted singlet, which lacked COSY correlations to other protons,

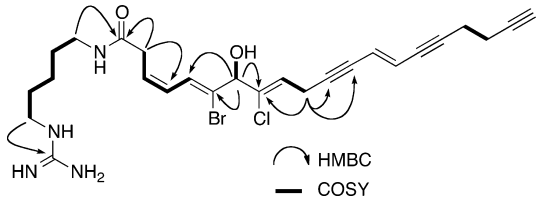

Figure 7. Key COSY and HMBC correlations of mollenyne D (**9**).

and the appearance of an additional vinyl proton signal (δ 6.08, t, J = 6.8 Hz) were consistent with a C-8–C-9 vinyl chloride with C-8 substituted by Cl. Last, the NOESY spectrum of **9** (Figures 3 and 7), showed cross-peaks linking H-5/H-7 and H-7/H-9 that confirmed the *Z* configuration to each of the Δ^5 and Δ^8 double bonds.

The formula, $C_{26}H_{32}BrClN_4O$, of mollenyne C (**8**) indicates a formal dehydrobromination product of **7**. NOESY cross-peaks between H-4 and H-7 in each compound (Figure 3) confirmed *E*-geometry to Δ^5, and no NOE correlations were observed between H-5 and H-7 in **8** and **10**. The relative stereoassignment of C-8 and C-9 in **8** is assumed to be *threo*, as in **7**, but because of limited sample, this remains a tentative assignment.

Introduction of the Δ^8 double bond in **9** and **10** results in near-degeneracy of ^{1}H and ^{13}C signals of H-/C-13 and H-/C-14 due to near-symmetry in the ene–yne segment. A second consequence of this change with respect to **6**–**8** is further insulation of the H-13/H-14 vinyl protons from their nearest neighbors. The integration of H-13/H-14 in **9** amounted to only 1.5 H under nominal NMR acquisition conditions (interscan delay of 1.0 s), which suggested poor spin–lattice relaxation efficiency and extraordinarily large longitudinal relaxation times (T_1), a consequence of unusually long interatomic distances to the nearest neighboring protons ($d \sim 5.4$ Å for H-13–H-9 or H-14–H-17, MMFF). The same phenomenon was evident in the ^{1}H NMR spectrum of **10**. Pulsed inversion recovery ^{1}H NMR experiments of the latter compound under ambient conditions (600 MHz, 25 °C; no attempt was made to remove dissolved O_2) revealed T_1 = 4.4 s for H-13/H-14 compared to a range of T_1 = 0.7–1.9 s for other sp^3 C–H signals and T_1 = 1.8 s for sp^2 C–H signals.

Biosynthetically, the likely precursor or precursors of the mollenynes are highly unsaturated poly ene–yne long-chain carboxylic acids, which are tailored by late-stage hydroxylation and halogenation events. It was surprising to find that the positions of Br and Cl in **6** and **7** are reversed at C-8 and C-9 and their relative configurations inverted, respectively. With the exception of **10**, mollenynes contain a C-7 allylic secondary hydroxyl group; presumably this is introduced through a cytochrome P_{450} mediated enzymatic oxidation of an unsaturated precursor, as is typical in the biosynthesis of similar allylic alcohols.[31] Assuming both **6** and **7** share the 7*S* absolute configuration (derived experimentally for **6**[13]), the implied relative configurations at C-8 and C-9 in **7** are epimeric to those stereocenters in **6**. The installation of vicinal Br and Cl atoms in **6** could occur through addition of an electrophilic "Br$^+$" equivalent to the *si* face of a putative *Z*-alkene precursor **i** followed by antiperiplanar backside attack by Cl$^-$ upon the resultant bromonium **ii** (Figure 8).[32] An intriguing possibility is that **6** may be a precursor of **7** through interchange of halogen positions through a type I dyotropic rearrangement,[33,34] a concerted "1,2-shift in which two migrating groups interchange their relative positions in a stationary scaffold".[34c] The consequence of passage of **6** through transition state **iii** is halogen interchange and double inversion at C-8 and C-9 in **7**. The structures of known

DOI: 10.1021/jacs.5b07858
J. Am. Chem. Soc. 2015, 137, 12343–12351

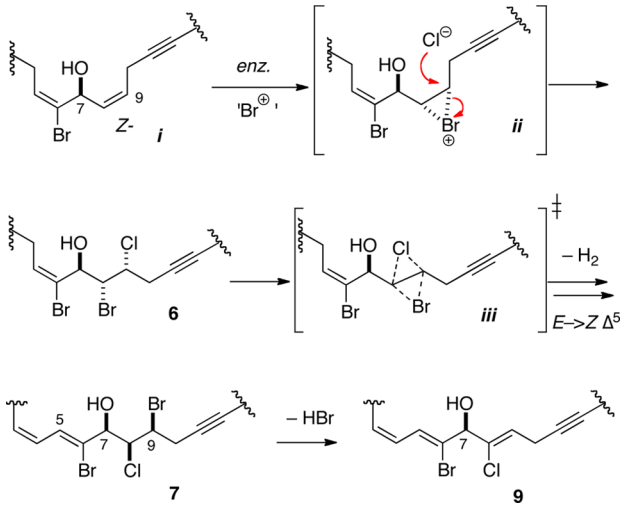

Figure 8. Hypothetical biosynthetic pathway to mollenynes A (**6**), B (**7**), and D (**9**).

chlorobromocyclohexane-containing natural products from red algae are also suggestive of involvement of a dyotropic rearrangement, for example, isocaespitol (**11**)[35] and caespitol (**12**)[36] from *Lawrencia caespitosa* Lamx, and other halogen-swapped isomeric pairs including the chamigranes obtusol, isoobtusol (also, *allo*-isoobtusol) from *L. cartilaginea*,[37] furocaespitane[38] and isofurocaespitane,[39] prepacifenol from *L. pacifica*, *L. johnstonni*, and *L. filiformis*,[40] and other related chamigranes.[41] Martin and co-workers demonstrated that crystalline **11**

Scheme 2. Thermal Rearrangement of Caespitol (11) to Isocaespitol (12)[a]

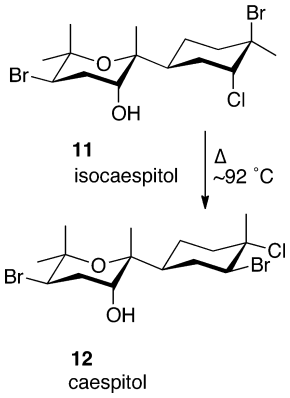

[a]See ref 35.

rearranges to the more stable diequatorial Br, Cl regioisomer **12** upon melting (Scheme 2)[35] and suggested rearrangement may also occur during extraction and isolation.[42] It is an open question whether dyotropic rearrangement occurs during the biosynthesis of **6**–**10** or whether the halogenase or another enzyme induces halogen exchange.[43] The intriguing possibility of existence of a "dyotropase" is a subject worthy of investigation in more detailed biosynthetic studies of mollenynes and related bromochloro compounds. Significantly, mollenyne B (**7**) has the correct configuration and conformation required for antiperiplanar β-elimination of HBr to give *Z*-Δ^8-**9**. Clearly other biosynthetic scenarios are possible (including regio- and stereo-random halogenations), but it is worth pointing out that the configurations of C-7–C-9 in **6** and **7**, as well as the Δ^8 double bond configuration of **9**, are unified under the former hypothesis.

Because of limited sample, it was not possible to assign absolute configuration of **7**–**9**. The CD spectra of **6**–**9** (see Supporting Information) were sufficiently different and complex to preclude a meaningful comparison or correlation.

CH_3OH extracts of almost all our samples of *Spirastrella mollis* exhibited antifungal activity against *Candida albicans* and other pathogenic yeasts; however, pure mollenyne A (**6**) was inactive (insufficient sample was available to assay **7**–**10**).[44]

CONCLUSIONS

Four new halogenated ene–ynes, mollenynes B–E (**7**-**10**), were isolated from the marine sponge *Spirastrella mollis* collected from Hogsty Reef, Bahamas, in nanomole yields, and their structures were elucidated through integrated interpretation of NMR, MS spectra, and computational chemistry. A useful variant of band-selective HSQC was developed that allowed indirect observation of $^{35}Cl/^{37}Cl$ isotope shifts in the ^{13}C dimension for location of Cl substituents on carbon frameworks and its application to natural products at the nanomole scale. Wider applications of this technique may include analysis of polyhalogenated terpenes and lipids from Rhodophyta (in particular, confirmation of constitution in equivocal assignments based on NMR) and MS-independent measurement of biosynthetic isotope fractionation in critical samples of rare natural products.

EXPERIMENTAL SECTION

General Experimental Procedures. Optical rotations were measured on a JASCO P-2000 polarimeter at the Na "double-D" emission line (λ of 589.0 and 589.3 nm) and reported here as $[\alpha]_D$. UV–vis spectra were measured on a JASCO V-630 spectrometer. FTIR spectra were collected on thin-film samples using a JASCO FTIR-4100 fitted with an ATR accessory (ZnSe plate). CD spectra were measured on a JASCO J-810 spectropolarimeter in quartz cells (1 or 5 mm path length). Inverse-detected 2D NMR spectra were measured on a JEOL ECA (500 MHz) spectrometer, equipped with a 5 mm $^1H\{^{13}C\}$ probe, or a Bruker Avance II (600 MHz) NMR spectrometer with a 1.7 mm $^1H\{^{13}C\}$ microcryoprobe. ^{13}C NMR spectra were collected on a Varian NMR spectrometer (125 MHz) equipped with a 5 mm Xsens $^{13}C\{^1H\}$ cryoprobe. NMR spectra were referenced to residual solvent signals (methanol-d_4, δ_H 3.31, δ_C 49.00 ppm; acetonitrile-d_3, δ_H 1.94 ppm), and submilligram yields were determined using the quantitation by solvent ^{13}C-satellites method (QSCS).[14a] High-resolution ESITOF analyses were carried out on an Agilent 1200 HPLC coupled to an Agilent 6350 TOFMS. Low-resolution MS measurements were made on a Thermoelectron Surveyor UHPLC coupled to an MSQ single-quadrupole detector. HPLC was performed on an Agilent 1100 HPLC.

Animal Material. The sponge *Spirastrella* sp. (11-25-40) was collected in 2011 at Hogsty Reef, Bahamas (latitude 21° 40.209′ N, longitude 073° 50.241′ W), at a depth of −28 m and stored at −20 °C until extraction. *Plocamium cartilagineum* was collected at low tide from Bird Rock, CA (latitude 32° 48.867′ N, longitude 117° 16.442′ W). Voucher samples of specimens are archived at University of California, San Diego.

Extraction and Isolation. The frozen lyophilized sponge (11-25-040) (235 g wet; 76 g dry wt) was extracted with CH_3OH at room temperature (500 mL × 2, 12 h), and the combined CH_3OH extracts were concentrated, and the water content was adjusted to approximately 1:9 H_2O/CH_3OH prior to repeated extraction with hexane (300 mL × 2). Concentration of the hexane-soluble layer gave fraction A (0.87 g). The aqueous-CH_3OH layer was adjusted to 2:3 H_2O/CH_3OH followed by extraction with CH_2Cl_2 (750 mL × 3). The combined CH_2Cl_2–CH_3OH layers were concentrated to yield fraction B (0.88 g). The aqueous layer was adjusted to approximately 9:1 H_2O/CH_3OH before extraction of the solution with *n*-BuOH (300 mL × 2). Concentration of

DOI: 10.1021/jacs.5b07858
J. Am. Chem. Soc. 2015, 137, 12343–12351

the combined *n*-BuOH-soluble partitions gave fraction C. Removal of the volatiles from the remaining aqueous phase provided fraction D. Fraction B was further purified by size exclusion chromatography (Sephadex LH-20, CH_3OH) to yield 11 fractions. The eighth fraction, 11-25-40B-F8 (50.1 mg), was purified by reversed phase HPLC (Phenomenex Luna C_{18} column, 250 mm × 10 mm, 4.0 mL·min^{-1}. Gradient: A, H_2O (0.1% TFA); B, CH_3CN; 0 min, 40% B; 2 min, 40% B; 20 min, 60% B) to afford four fractions. The first fraction (t_R = 13.74 min, 0.90 mg) was further purified by reversed phase HPLC (Phenomenex Luna C_{18}(2) column, 250 mm × 10 mm, 3.5 mL·min^{-1}. Gradient: A, H_2O (0.1% TFA); B, CH_3CN; 0 min, 60% B; 2 min, 60% B; 20 min, 80% B) to afford mollenyne D (**9**) (t_R = 17.12 min, 13 μg, 0.17 ppm yield based on dry wt). The second fraction (t_R = 14.06 min, 0.72 mg) was further purified by reverse phase HPLC (Phenomenex Luna C_{18}(2) column, 250 mm × 4.6 mm, 1.0 mL·min^{-1}. Gradient: A, H_2O (0.1% TFA); B, CH_3OH; 0 min, 50% B; 2 min, 50% B; 30 min, 90% B) to afford mollenyne B (**7**) (t_R = 8.14 min, 43 μg, 0.57 ppm yield). The third fraction (t_R = 17.17 min, 0.66 mg) was further purified by reversed phase HPLC (Phenomenex Luna C_{18}(2) column, 250 mm × 10 mm, 3.5 mL·min^{-1}. Gradient: A, H_2O (0.1% TFA); B, CH_3CN; 0 min, 70% B; 2 min, 70% B; 20 min, 90% B) to afford mollenyne E (**10**) (t_R = 11.93 min, 12 μg, 0.16 ppm yield). The fourth fraction (t_R = 18.82 min, 0.72 mg) was further purified by reversed phase HPLC (Phenomenex Luna C_{18}(2) column, 250 mm × 10 mm, 3.5 mL·min^{-1}. Gradient: A, H_2O (0.1% TFA); B, CH_3CN; 0 min, 70% B; 2 min, 70% B; 20 min, 90% B) to afford mollenyne C (**8**) (t_R = 15.23 min, 20 μg, 0.26 ppm yield).

Frozen *P. cartilagineum* (252.2 g) was homogenized in CH_2Cl_2–MeOH (800 mL) at room temperature using a high-speed blender. The dark green suspension was filtered through filter paper (Whatman grade 1) contained in a Büchner funnel, and the clear dark green aqueous-MeOH was concentrated to give a dark-green oil (1.02 g) that was was subjected to further fractionation by automated gradient flash chromatography (25–100% hexanes–CH_2Cl_2; CH_2Cl_2–MeOH 0–10%). Earlier eluting fractions containing UV-active material (TLC) were pooled and further separated by repeated HPLC (normal silica phase, silica, 5 μm, 10 mm × 250 mm, elution with isooctane and hexanes; reversed phase, C_{18}, 5 μm, 10 mm × 250 mm, elution with 80:20 CH_3CN–H_2O). Each peak eluate from HPLC was extracted with distilled pentane. Removal of solvent from the extracts delivered several known polyhalogenated terpenes[4] including pure **1b**.

(1*Z*,3*E*,5*S,6*R**,7*E*)-8-Bromo-1,5,6-trichloro-2-(dichloromethyl)-6-methylocta-1,3,7-triene (1b).** Clear oil. The ^{1}H NMR and MS data of **1b** matched the literature values (see "compound **10**" of Mynderse and Faulkner).[4] Complete ^{1}H and ^{13}C NMR assignments, here, are based on 2D NMR including bsHSQC. ^{1}H NMR (600 MHz, $CDCl_3$) δ 6.97 (s, 1H, H10), 6.57 (d, J = 13.6 Hz, 1H, H8), 6.45 (d, J = 13.6 Hz, 1H, H7), 6.36 (m*, 1H, H3), 6.34 (m*, 1H, H4), 6.32 (s*, 1H, H1), 4.54 (d, J = 7.4 Hz, 1H, H5), 1.77 (s, 3H, H9) (∗ indicates overlapped signals); ^{13}C NMR ($CDCl_3$) δ 138.5 (CH, C-7), 137.5 (C_q, C-2), 129.6 (CH, C-4), 127.4 (CH, C-3), 119.6 (CH, C-1), 110.2 (CH, C-8), 71.5 (C_q, C-6), 68.2 (CH, C-5); ^{13}C NMR (125 MHz, $CDCl_3$) δ 138.5 (CH, C-7), 137.5 (C_q, C-2), 129.6 (CH, C-4), 127.4 (CH, C-3), 119.6 (CH, C-1), 110.2 (CH, C-8), 71.5 (C_q, C-6), 68.2 (CH, C-5), 65.5 (CH, C-10), 25.3 (CH_3, C-9).

Mollenyne B (7). Colorless solid. UV (CH_3OH, 23 °C) λ_{max} (log ε) 253 (4.59), 260 (4.61), 275 (4.44) nm. CD (CH_3OH, 23 °C) λ 243 nm ($\Delta\varepsilon$ = +13.2), 262 (−22.5). See Tables 1 and 2 for ^{1}H and ^{13}C NMR data. HRESIMS m/z 627.0728 $[M + H]^+$ (calcd for $C_{26}H_{34}Br_2ClN_4O_2$, 627.0732).

Mollenyne C (8). Colorless solid. UV (CH_3OH, 23 °C) λ_{max} (log ε) 253 (4.49), 260 (4.51), 275 (4.35) nm. CD (CH_3OH, 23 °C) λ 248 nm ($\Delta\varepsilon$ = +4.0), 266 (−5.7). See Tables 1 and 2 for ^{1}H and ^{13}C NMR data. HRESIMS m/z 611.0772 $[M + H]^+$ (calcd for $C_{26}H_{34}Br_2ClN_4O$, 611.0782).

Mollenyne D (9). Colorless solid. UV (CH_3OH, 23 °C) λ_{max} (log ε) 254 (4.52), 260 (4.55), 275 (4.38) nm. CD (CH_3OH, 23 °C) λ 229 nm ($\Delta\varepsilon$ = −0.4), 253 (+3.0). See Tables 1 and 2 for ^{1}H and ^{13}C NMR data. HRESIMS m/z 547.1467 $[M + H]^+$ (calcd for $C_{26}H_{33}BrClN_4O_2$, 547.1470).

Mollenyne E (10). Colorless solid. UV (CH_3OH, 23 °C) λ_{max} (log ε) 253 (4.70), 260 (4.73), 275 (4.58) nm. See Tables 1 and 2 for ^{1}H and ^{13}C NMR data. HRESIMS m/z 531.1513 $[M + H]^+$ (calcd for $C_{26}H_{33}BrClN_4O$, 531.1521).

Antifungal Disk Diffusion Assay. An overnight liquid culture of *C. albicans* ATCC 14503 was diluted 100-fold and spread on Mueller–Hinton agar plates. Aliquots of each compound (100 μg) were applied as solutions in DMSO onto sterile paper disks (6.0 mm). After 5 min, the disks were placed on the yeast-coated agar plates and incubated overnight at 35 °C. Antifungal activity was estimated by measurement of zones of inhibition (>6.0 mm, ±0.5 mm).

Molecular Mechanics Calculations. Simple interatomic distances and bond angles were determined from MMFF calculations (Spartan '14, Wavefunction, Irvine, CA). Energies and conformations were calculated using molecular mechanics (MMFF) or, more accurately, using semiempirical (Hartree–Fock) or DFT methods (Gaussian 09, Gaussian Inc., Wallingford, CT). Calculations of NMR homonuclear ^{1}H spin–spin coupling constants (DU8)[25] and ^{1}H and ^{13}C chemical shifts (DP4)[30] were carried out as detailed in the references using molecule geometries obtained from MMFF and refined by DFT calculations. See Supporting Information for details.

■ ASSOCIATED CONTENT

Supporting Information

The Supporting Information is available free of charge on the ACS Publications website at DOI: 10.1021/jacs.5b07858.

^{1}H, ^{13}C NMR and 2D NMR spectra of **7**–**10**, CD spectra, and DFT calculations of model compounds (PDF)

■ AUTHOR INFORMATION

Corresponding Author

*tmolinski@ucsd.edu

Notes

The authors declare no competing financial interest.

■ ACKNOWLEDGMENTS

We thank P. Stout (UCSD) for assistance with collection of *Spirastrella mollis* and S. Zea (Universidad Nacional de Colombia, InveMar) for taxonomic identification, M. Jamison (UCSD) for antifungal assay results, T. Cheng and L. Januar (UCSD) for assistance with purification of compounds, and an anonymous reviewer for suggestions on DP4 calculations. We thank the Government of the Bahamas for permission to collect samples through an unnumbered permit for operations in their territorial waters, and J. R. Pawlik (University of North Carolina, Wilmington) and the captain and crew of the R/V Walton Smith for expedition logistics. We are grateful to Y. Su for measurements of HRMS, and A. Mrse (UCSD) for assistance with additional NMR measurements. The 500 MHz NMR spectrometer and the HPLC TOF mass spectrometer were purchased with funds provided by the NSF (Chemical Research Instrument Fund, Grant CHE0741968) and the NIH (Shared Instrument Grant S10RR025636), respectively. This work was supported by a grant from NIH (Grant AI1007786).

■ REFERENCES

(1) (a) Gribble, G. W. *Acc. Chem. Res.* **1998**, *31*, 141–152. (b) Hartung, J. *Angew. Chem., Int. Ed.* **1999**, *38* (9), 1209–1211. (c) Gribble, G. W. *J. Chem. Educ.* **2004**, *81*, 1441–1449.

(2) Gribble, G. W. *Mar. Drugs* **2015**, *13*, 4044–4136.

(3) (a) The originally proposed structure of **1** was incorrectly assigned with interchanged Br and Cl substituents but later corrected by an X-ray crystal structure: Mynderse, J. S.; Faulkner, D. J. *J. Am. Chem. Soc.* **1974**, *96*, 6771. (b) van Engen, D.; Clardy, J.; Kho-Wiseman, E.; Crews, P.; Higgs, M. D.; Faulkner, D. J. *Tetrahedron Lett.* **1978**, *19*, 29–32.

(4) Mynderse, J. S.; Faulkner, D. J. *Tetrahedron* **1975**, *31*, 1963–1967.

DOI: 10.1021/jacs.5b07858
J. Am. Chem. Soc. 2015, 137, 12343–12351

(5) D'Ambrosio, M.; Guerriero, A.; Pietra, F. *Helv. Chim. Acta* **1984**, *67*, 1484−1492.
(6) Lacy, C.; Scheuer, P. J. *J. Nat. Prod.* **2000**, *63* (1), 119−121.
(7) Shen, S.; Liu, D.; Wei, C.; Proksch, P.; Lin, W. *Bioorg. Med. Chem.* **2012**, *20* (24), 6924−6928.
(8) Lee, Y.-J.; Han, S.; Lee, H.-S.; Kang, J. S.; Yun, J.; Sim, C. J.; Shin, H. J.; Lee, J. S. *J. Nat. Prod.* **2013**, *76* (9), 1731−1736.
(9) Urban, S.; de Almeida Leone, P.; Carroll, A. R.; Fechner, G. A.; Smith, J.; Hooper, J. N. A.; Quinn, R. J. *J. Org. Chem.* **1999**, *64*, 731−735.
(10) (a) Grube, A.; Köck, M. *Angew. Chem., Int. Ed.* **2007**, *46* (13), 2320−2324.
(11) (a) Teruya, T.; Nakagawa, S.; Koyama, T.; Arimoto, H.; Kita, M.; Uemura, D. *Tetrahedron* **2004**, *60*, 6989−6993. (b) Gao, S.; Wang, Q.; Chen, C. *J. Am. Chem. Soc.* **2009**, *131*, 1410−1412.
(12) Skepper, C. K.; Molinski, T. F. *J. Org. Chem.* **2008**, *73*, 2592−2597.
(13) Morinaka, B. I.; Molinski, T. F. *Org. Lett.* **2011**, *13*, 6388−6341.
(14) (a) Dalisay, D. S.; Molinski, T. F. *J. Nat. Prod.* **2009**, *72*, 739−744. (b) Molinski, T. F. *Nat. Prod. Rep.* **2010**, *27*, 321−329. (c) Dalisay, D. S.; Rogers, E. W.; Edison, A.; Molinski, T. F. *J. Nat. Prod.* **2009**, *72*, 732−738. (d) Molinski, T. F. *Curr. Opin. Drug Discovery Dev.* **2009**, *12*, 197−206.
(15) Kozminski, W.; Nanz, D. *J. Magn. Reson.* **2000**, *142*, 294−299.
(16) Matsumori, N.; Kaneno, D.; Murata, M.; Nakamura, H.; Tachibana, K. *J. Org. Chem.* **1999**, *64*, 866−876.
(17) (a) Sergeyev, N. M.; Sergeyeva, N. D.; Raynes, W. T. *Magn. Reson. Chem.* **1994**, *32*, 381−385. (b) Buchner, W.; Scheutzow, D. *Org. Magn. Reson.* **1975**, *7*, 615−616. (c) Aliev, A. E.; Harris, K. D. M. *Magn. Reson. Chem.* **1993**, *31*, 54−57. (d) Sergeyev, N. M.; Sandor, P.; Sergeyeva, N. D.; Raynes, W. T. *J. Magn. Reson., Ser. A* **1995**, *115*, 174−182. (e) Foris, A. *Magn. Reson. Chem.* **2000**, *38*, 813−819. (f) Hu, D. X.; Seidl, F. J.; Bucher, C.; Burns, N. Z. *J. Am. Chem. Soc.* **2015**, *137*, 3795−3798.
(18) Raynes, W. T.; Grayson, M.; Sergeyev, N. M.; Sergeyeva, N. D. *Chem. Phys. Lett.* **1994**, *226*, 433−439.
(19) Poppe, L.; van Halbeek, H. *Magn. Reson. Chem.* **1991**, *29*, 848−851.
(20) The ^{13}C window was adjusted to minimize "fold-back".
(21) NMR Periodic Table. http://www.bruker-nmr.de/guide/eNMR/chem/Cl.html.
(22) It is generally accepted that the absolute $^{37}Cl/^{35}Cl$ isotope ratio in ocean waters (but not ground water) is uniform and invariant. The primary standard "halite", NIST SRM 975, is 0.31977 ± 0.00081 2σ, Shields, W. S.; Murphy, T. J.; Garner, E. L.; Dibeler, V. H. *J. Am. Chem. Soc.* **1962**, *84*, 1519−1522. An accurately calibrated secondary standard, derived from seawater from a different location (ISL 354), differs only slightly from the former (δ −0.39 ± 0.05‰ 2σ); see Xiao, Y. K.; Zhou, Y.; Wang, Q.; Wei, H.; Liu, W.; Eastoe, C. J. *Chem. Geol.* **2002**, *182*, 655−661. Our value of 0.30 ± 0.05 is slightly lower than NIST SRM 975 (δ −62‰) and ISL 354; however, the $^{37}Cl/^{35}Cl$ ratio may be altered in mollenynes and other chlorinated marine natural products because of isotopic fractionation during their biosynthesis.
(23) Kaupp, M.; Malkin, O. L.; Malkin, V. G. *Chem. Phys. Lett.* **1997**, *265*, 55−59.
(24) Kurz, M.; Schmieder, P.; Kessler, H. *Angew. Chem., Int. Ed. Engl.* **1991**, *30*, 1329−1331.
(25) (a) Kutateladze, A. G.; Mukhina, O. A. *J. Org. Chem.* **2014**, *79*, 8397−8406. (b) Kutateladze, A. G.; Mukhina, O. A. *J. Org. Chem.* **2015**, *80*, 5218−25.
(26) (a) Wiitala, K. W.; Hoye, T. R.; Cramer, C. J. *J. Chem. Theory Comput.* **2006**, *2*, 1085−1092. (b) Lodewyk, M. W.; Siebert, M. R.; Tantillo, D. J. *Chem. Rev.* **2012**, *112*, 1839−62. (c) Willoughby, P. H.; Jansma, M. J.; Hoye, T. R. *Nat. Protoc.* **2014**, *9*, 643−660.
(27) Small differences between measured and calculated *J* values are possibly due to imperfect conformer weightings in the DFT calculations (see ref 25b).
(28) (a) Barone, G.; Gomez-Paloma, L.; Duca, D.; Silvestri, A.; Riccio, R.; Bifulco, G. *Chem. - Eur. J.* **2002**, *8*, 3233−3239. (b) Barone, G.; Duca, D.; Silvestri, A.; Gomez-Paloma, L.; Riccio, R.; Bifulco, G. *Chem. - Eur. J.* **2002**, *8*, 3240−3245.
(29) Pankratyev, E. Y.; Tulyabaev, A. R.; Khalilov, L. M. *J. Comput. Chem.* **2011**, *32*, 1993−1997.
(30) Smith, S. G.; Goodman, J. M. *J. Am. Chem. Soc.* **2010**, *132*, 12946−12959.
(31) Schneider, C.; Schreier, P.; Humpf, H.-U. *Chirality* **1997**, *9*, 563−567.
(32) We favor bromonium ion formation (**ii**) by attack of Br^+ on the alkene followed by displacement by Cl^- rather than the reverse because most marine derived halogenated marine natural products appear to arise from electrophilic attack by Br^+ species (lower oxidation potential of Br^-). This is supported by literature; the few, well-characterized "halogenases" from marine organisms responsible for electrophilic halogenation are all bromoperoxidases, not chloroperoxidases: Butler, A.; Carter-Franklin, J. N. *Nat. Prod. Rep.* **2004**, *21*, 180−188. Although a slight preference for attack of Cl^- at the electron-poor C-8 rather than C-9 in **ii** might be expected, the putative outcome presented in Figure 3 is not necessarily counterintuitive if dihalogenation is directed by a "halogenase" enzyme that orchestrates not only diastereoselectivity but also regioselectivity. Interestingly, we found that electrophilic addition of BrCl to a model compound (*Z*-(*tert*-butyldimethylsilyoxy)-2-hexene, **iv**, hexane, 23 °C) favored the *erythro*-8-bromo-9-chloro-7-alkanol **v** over regioisomeric *erythro*-**vi** (mollenyne numbering, 4:1 ratio);

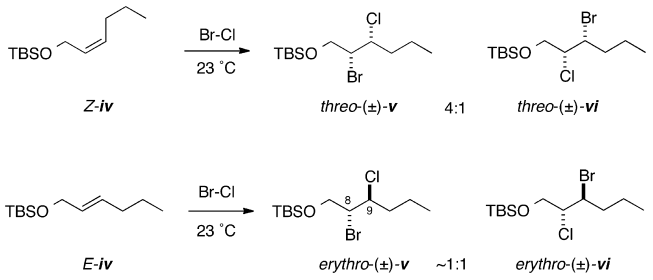

however, under the same conditions *E*-**iv** gave an equimolar mixture of regioisomers *threo*-**v** and *threo*-**vi** (manuscript in preparation).

(33) Reetz, M. T. *Angew. Chem., Int. Ed. Engl.* **1972**, *11*, 129−130.
(34) (a) Grob, C. A.; Winstein, S. *Helv. Chim. Acta* **1952**, *35*, 782−802. (b) Barton, D. H. R.; Head, A. J. *J. Chem. Soc.* **1956**, 932−937. (c) Alt, G. H.; Barton, D. H. R. *J. Chem. Soc.* **1954**, 4284−4294. (d) Fernandez, I.; Cossio, F. P.; Sierra, M. A. *Chem. Rev.* **2009**, *109*, 6687−6711.
(35) González, A. G.; Derias, J.; Martín, J. D.; Perez, C. *Tetrahedron Lett.* **1974**, *15*, 1249−1250.
(36) González, A. G.; Darias, J.; Martín, J. D. *Tetrahedron Lett.* **1973**, *14*, 2381−2384.
(37) Juagdan, E. G.; Kalidindi, R.; Scheuer, P. J. *Tetrahedron* **1997**, *53*, 521−528.
(38) González, A. G.; Darias, J.; Martín, J. D. *Tetrahedron Lett.* **1973**, *14*, 3625−3626.
(39) González, A. G.; Martín, J. D.; Martin, V. S.; Norte, M. *Tetrahedron Lett.* **1979**, *20*, 2719−2722.
(40) Sims, J. J.; Fenical, W.; Wing, R. M.; Radlick, P. *J. Am. Chem. Soc.* **1973**, *95*, 972−972.
(41) Elsworth, J. F.; Thomson, R. H. *J. Nat. Prod.* **1989**, *52*, 893−895.
(42) In our hands, attempted thermal rearrangement of 7 resulted only in decomposition.
(43) It is unlikely that Cl and Br halogen exchange by type 1 dyotropic rearrangements is spontaneous at ambient temperatures in the biosynthesis of the natural products, as the energy of activation E_a would appear to be too high. Dyotropic rearrangements of cyclic dihalogenated cyclohexanes only occurred at or above melting temperatures, for example, 2β,3α-dibromocholestane, mp 144−145 °C (Hattori, K.; Kawasaki, C. *J. Pharm. Soc. Jpn.* **1937**, *57*, 115, 588), or after 30 min at 200 °C (ref 34c), and Martin's bromochloro-containing caespitol (mp 92−93 °C, ref 35).
(44) The antifungal activity of the extracts was traced to other components in "fraction B" obtained from the solvent partitioning of the crude CH_3OH extract. The latter observations will be the subject of another report.

DOI: 10.1021/jacs.5b07858
J. Am. Chem. Soc. 2015, 137, 12343−12351